

Original Research

Performance of Tetracycline Hydrochloride Removal Using Acidized and Magnetized Waterworks Sludge as Adsorbent

Jingxi Tie¹, Huidong Zhang¹, Xiaohan Duan², Shuo Sang¹, Weipeng Li¹,
Minghua Wei^{3,4*}, Zhihong Zheng^{5**}

¹School of Environmental and Municipal Engineering, North China University of Water Resources and Electric Power, Zhengzhou, 450045, China

²School of Water Conservancy, North China University of Water Resources and Electric Power, Zhengzhou 450046, China

³School of water resource, North China University of Water Resources and Electric Power, Zhengzhou, 450045, China

⁴Henan Key Laboratory of Water Resources Conservation and Intensive Utilization in the Yellow River Basin, Zhengzhou, 450046, China

⁵Henan Vocational College of Water Conservancy and Environment, Zhengzhou, 450008, China

Received: 1 July 2022

Accepted: 19 June 2022

Abstract

The current disposal of waterworks sludge (WS) by landfill or discharge into water body results in land consumption and environment pollution. To solve the problem, alum-based waterworks sludge (AWS) was reclaimed and reused to develop adsorbent for aqueous tetracycline hydrochloride (TCH) removal. WS was modified using HCl solution and Fe²⁺/Fe³⁺ coprecipitation to get acidized and magnetized waterworks sludge (Fe₃O₄@HAWS) for the improvement of its adsorption capacity and separation efficiency. Fe₃O₄@HAWS was used as adsorbent to test its static TC adsorption performance. The results suggested that the TCH adsorption was a pH dependent process, and the maximum TCH adsorption by Fe₃O₄@HAWS was achieved at pH 5 at 25°C in the pH range of 3-10. Among the three kinetic models, the pseudo-second-order equation best characterized the adsorption process, while the Freundlich equation best described the adsorption process. The thermodynamic study indicated that the adsorption process was spontaneous and exothermic. The investigation demonstrated that the composite was successful for aqueous TCH adsorption and spent adsorbent separation, providing not only a unique notion for the sustainable and environmentally friendly treatment and disposal of WS, but also a novel solution for TCH-containing wastewater treatment.

Keywords: acidized and magnetized waterworks sludge (Fe₃O₄@HAWS), tetracycline hydrochloride (TCH), adsorption

*e-mail: wmh@ncwu.edu.cn

**e-mail: zzh_ncwu@163.com

Introduction

Antibiotics have been developed and used for microorganism-related diseases for both human and animal successfully, with an annual consumption of about 10^5 - 2×10^5 tons globally [1, 2]. Among the antibiotic, tetracyclines (TCs) are ranked second globally whereas first in China both in term of production and consumption [3-5].

TCs are widely applied for disease therapy and livestock feed due to their broad-spectrum resistance to various kinds of pathogenic bacteria [6, 7]. However, only a very little fraction of the TCs can be absorbed or metabolized by living organisms because of its stable structure and strong anti-degradation [8, 9], and the majority of TCs intake are released into the environment through urine and feces [9, 10]. As a result, a large quantity of TCs has been released into the environment via drug manufacturing wastewater, animal and agricultural wastes [11], resulting in bacterial resistance and high antibiotic resistance risk [12-14], and exposure to antibiotic could lead to metabolic and immune diseases [15, 16]. Hence, it is critical to remove TCs from wastewater before it is dumped into water bodies.

For TCs-bearing wastewater treatment, a variety of approaches have been tried, including advanced oxidation processes [4, 17, 18], bio-degradation [19], adsorption and membrane technology [20-23]. Adsorption is acknowledged as an efficient technique for TCs removal due to its merits including easy operation, tiny secondary pollution, low cost and low energy consumption [24]. Adsorbents with a cheap cost and high capacity are essential for adsorption technology use.

Coagulation/flocculation is a very important procedure for drinking water production in surface water treatment plants all over the world. Inorganic coagulant, including alum-based and iron-based coagulants are widely used for turbidity removal from raw water globally [15, 25]. The flocs generated by the hydrolyzed coagulants with the suspended solid and colloid settle in the sedimentation tank, resulting in a massive amount of waterworks sludge (WS) including alum-based WS (AWS) and iron-based WS (IWS) on a global scale [19, 26, 27]. Hydrolyzed coagulants, silica, clay minerals, and dissolved organic materials are common constituents of WS [28]. The expenses of WS disposal are enormous and continue to rise as rules become tighter [29].

The recycling and reuse of the WS is a feasible alternative to solve the problem of WS disposal, and the WS has been used for coagulant recovery and reuse [30], sewage sludge dewatering [31], clay brick and concrete production [32, 33]. Additionally, WS has been confirmed to be effective for pollutant adsorption due to its abundant active components transformed from the coagulant. For instance, Hou et al. reported that four kinds of alum sludge collected from different water treatment plants had phosphorus adsorption ranging

from 2.06 to 6.06 mg/g, which was affected by the Al and Ca contents and initial phosphorus concentration [34]. Hak et al. used the adsorbent prepared by the hydrothermal treatment of ABWS obtained from a water treatment plant for fluoride and arsenic removal from water, with the maximum adsorption of 7.6 and 5.6 mg/g for fluoride and arsenic, respectively [35]. Our previous study found that IWS treated with 1 mol/L H_2SO_4 had the highest phosphorus adsorption capacity of 4.79 mg/g when compared to the raw IWS and IWS treated with 0.5, 2 and 3 mol/L H_2SO_4 [36]. Besides, WS was also found effective for the removal of other pollutants such as As(V), Mo(VI) and dyes, etc. [37-39].

Despite the successful adsorption of various pollutants, challenging separation of sludge from the solution following adsorption limits its practical applicability. Magnetization has been used successfully to increase particle adsorbent separation from water. For instance, Zou et al. synthesized magnetic bentonite and used it to remove Pb(II) from water. The spent adsorbent could be easily removed from the solution due to its superparamagnetic nature [41]. There has been very little study on TCH adsorption utilizing magnetized WS.

As a result, AWS was activated by HCl and magnetized using Fe^{2+}/Fe^{3+} coprecipitation in sequence to increase its pollutant adsorption and facilitate its separation from water, allowing AWS to be reused in a unique method and providing fresh insight into TCH removal. In this investigation, the produced composite was utilized as an adsorbent to remove TCH from its aqueous solution. pH, reaction duration, and temperature were explored as influencing variables.

Experimental

Preparation of HCl modified AWS (HAWS)

WS used in this study was collected from a drinking water treatment plant in Zhengzhou, China, which was dried in the open air for several days before being dried in a drier at 105°C for 2 h. The dried WS was crushed and passed through 0.15 mm screen mesh. 10 g AWS was combined with 20 mL HCl solution at a concentration of 1.0-3 mol/L, and ultrasonically treated for 5 min. To get the HAWS, the slurry was centrifuged, rinsed with deionized water, and dried at 105°C to get the HAWS.

Magnetized HAWS ($Fe_3O_4@HAWS$) was prepared using the Fe^{2+}/Fe^{3+} coprecipitation described in the publication. In particular, 20 g (S1), 10 g (S2), 5 g (S3), 2.5 g (S4), 1.25 g (S5), and 0 g HAWS (pure Fe_3O_4), 6.3 g $FeCl_3 \cdot 6H_2O$ and 4.2 g $FeCl_2 \cdot 7H_2O$ were combined in 100 mL of deionized water in a three-necked flask in water bath with vigorous stirring. When the temperature of the water bath reached 90°C, 10 ml of ammonia was promptly added to the mixture, and the mixture was reacted for 1 h at that temperature. To get

$\text{Fe}_3\text{O}_4@\text{HAWS}$, the black precipitate was recovered, washed multiple times with deionized water, and dried at 50°C.

Characterization

The X-ray fluorescence (XRF, Smartlab 3kw, Rigaku Ltd., Japan) was used to analyze the compositions of AWS, HAWS and $\text{Fe}_3\text{O}_4@\text{HAWS}$. XRD patterns of AWS, HAWS and $\text{Fe}_3\text{O}_4@\text{HAWS}$ were acquired with an X-ray diffractometer (Smartlab 3kw, Rigaku Ltd., Japan). FTIR spectra of HAWS, $\text{Fe}_3\text{O}_4@\text{HAWS}$ before and after TCH adsorption were obtained using a FTIR spectrum (Nicolet 5700, thermo Nicolet Ltd., USA) to investigate the surface functional groups. The surface area of AWS, HAWS and $\text{Fe}_3\text{O}_4@\text{HAWS}$ was measured using N_2 adsorption isotherm with a model of Brunauer, Emmett, and Teller (Autosorb-I, Quantachrome, USA). The zero point charge (pH_{PZC}) was measured using the approach [42]: In conical flasks, 25 mL of NaCl solution (0.1 mol/l) with pH values ranging from 3 to 10 were combined with 0.05 g $\text{Fe}_3\text{O}_4@\text{HAWS}$. The conical flasks were shaken at 150rpm in a shaker for 48h at 25°C. The mixtures were filtered through 0.45 μm , and the pH of the resulting solution was determined using pH meter (pHs-3c, INESA Scientific Instrument Co., Ltd., China). The ΔpH between the final pH and the initial pH was plotted against the initial pH. The pH_{PZC} of $\text{Fe}_3\text{O}_4@\text{HAWS}$ was defined as the intersection of the curve and the horizontal line of $\Delta\text{pH} = 0$.

Preparation of the Artificial Wastewater

The wastewater used in the experiment was synthesized by adding tetracycline hydrochloride (TCH, molecular structure in Fig. 1) in the deionized water, and the pH value of the wastewater was adjusted using 0.1 mol/L HCl and NaOH solutions.

Adsorption Studies

Batch adsorption experiment was carried out in the following way: 0.01g of $\text{Fe}_3\text{O}_4@\text{HAWS}$ was mixed with 20 mL of TCH solution in conical flask. The mixture was reacted in a shaker at 120 rpm for various time intervals. The mixture was centrifuged at 2000 rpm for 5 min before being filtered through a 0.45 μm

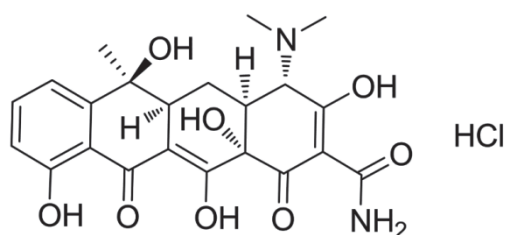


Fig. 1. The molecular structure of TCH.

membrane filter. A UV-Vis spectrophotometer (UV-5100, Yuanxi Instruments, Shanghai, China) was used to measure the residual TCH content in the filtrate at 358 nm. The quantity of TCH adsorbed by $\text{Fe}_3\text{O}_4@\text{HAWS}$ was determined using the following equation:

$$q = \frac{(C_0 - C_e)V}{m} \quad (1)$$

where q was the amount of TCH adsorbed (mg/g), C_0 and C_e were the initial and the equilibrium concentration of TCH (mg/L), respectively, V was the volume of solution (L) and m was the $\text{Fe}_3\text{O}_4@\text{HAWS}$ mass (g) used for the experiment.

Results and Discussion

Determination of the Best Condition for $\text{Fe}_3\text{O}_4@\text{HAWS}$ Preparation

As shown in Fig. 2a) and 2b), HAWS treated using 2.5 mol/L HCl for 10 min had the highest TCH removal of 92.74 mg/g and 48.18 mg/g, respectively. $\text{Fe}_3\text{O}_4@\text{HAWS}$ produced with varying HAWS doses (S1-S5) performed better for TCH adsorption than HAWS and pure Fe_3O_4 (S6) for TCH adsorption, and S1 had the best TCH adsorption of 65.06 mg/g (Fig. 2c). Meanwhile, S1 exhibited the third largest saturation magnetic induction of 23.99 emu/g among the six samples, making separation from solution easier (Fig. 2d). As a result, the optimal condition for $\text{Fe}_3\text{O}_4@\text{HAWS}$ preparation was the WS modified with 2.5mol/L HCl for 10 min to get the HAWS, and 5 g HAWS and 6.3 g $\text{FeCl}_3 \cdot 6\text{H}_2\text{O}$ and 4.2 g $\text{FeCl}_2 \cdot 7\text{H}_2\text{O}$ was used to prepare $\text{Fe}_3\text{O}_4@\text{HAWS}$, which was used to carry out the following study.

Characterization of the Material

As shown in Table 1, AWS, HAWS and $\text{Fe}_3\text{O}_4@\text{HAWS}$ contained abundant SiO_2 , which came from the inorganic solid in the raw water. Coagulants employed in the waterworks for drinking water purification were the main source of Al_2O_3 and Fe_3O_4 in AWS. Calcium oxide content decreased from 11.98% for WS to 0.72% for HAWS due to HCl dissolution. After modification using $\text{Fe}^{2+}/\text{Fe}^{3+}$ coprecipitation, the Fe_3O_4 content of $\text{Fe}_3\text{O}_4@\text{HAWS}$ increased to 42.46% dramatically. The S_{BET} and the total pore volume of HAWS increased from 31.48 m^2/g to 35.88 m^2/g , and from 0.017 cm^3/g to 0.020 cm^3/g after HCl treatment, respectively, and the two parameters of $\text{Fe}_3\text{O}_4@\text{HAWS}$ were greatly enlarged after modification using $\text{Fe}^{2+}/\text{Fe}^{3+}$ coprecipitation, which was favorable for the adsorption process.

As shown in Fig. 3a), the raw WS contained quartz, calcite and albite. After treatment by HCl, the diffraction peaks of calcite largely vanished for

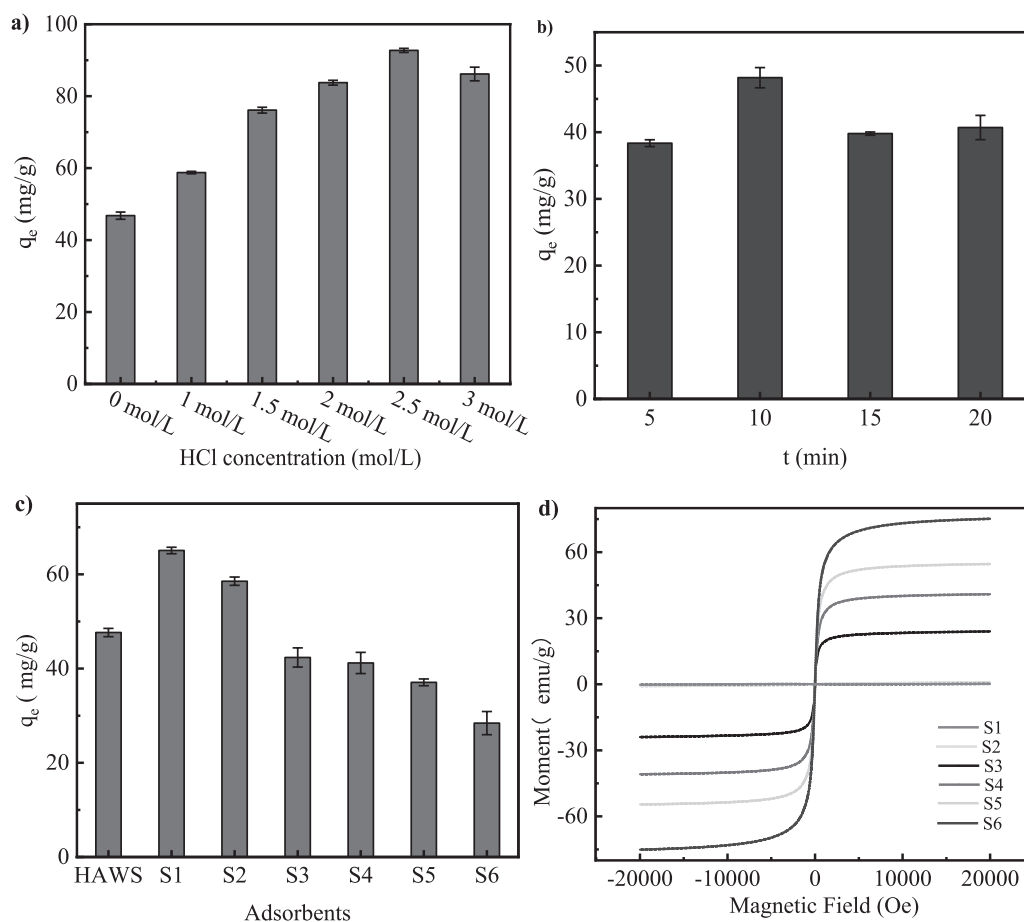


Fig. 2. Determination of the best condition for Fe₃O₄@HAWs preparation: effect of HCl concentration on TCH adsorption by HAWS a) ($C_0 = 25$ mg/L, Temperature = 35°C, reaction time = 24 h); effect of HCl treatment time on TCH adsorption by HAWS ($C_0 = 25$ mg/L, Temperature = 15°C, reaction time = 24 h); effect of ratio of Fe₃O₄ to HAWS on TCH adsorption by Fe₃O₄@HAWs ($C_0 = 25$ mg/L, Temperature = 25°C, reaction time = 24 h); VSM curve of Fe₃O₄@HAWs at different ratio of Fe₃O₄ to HAWS.

HAWs, which was consistent with the result obtained from XRF analysis. The diffraction peaks of magnetite occurred in the spectra of Fe₃O₄@HAWs at $2\theta = 30.4^\circ$, 35.8° , 43.5° , 54° , 57.5° and 63° , indicating the successful modification using Fe²⁺/Fe³⁺ coprecipitation.

As shown in Fig. 3b), the peaks at 3454 cm^{-1} and 1637 cm^{-1} belonged to the vibration of -OH for HAWs [43, 44], and the peaks at 1035 cm^{-1} belonged to Si-O-Si stretching [45]. In contrast to HAWs, the peaks of -OH of Fe₃O₄@HAWs shifted to 3442 cm^{-1} and the peaks

Table 1. Main compositions, specific areas and total pore volumes of AWS, HAWs and Fe₃O₄@HAWs.

Compositions	Oxide percentage (%)		
	AWS	HAWs	Fe ₃ O ₄ @HAWs
SiO ₂	32.35	41.86	26.69
Al ₂ O ₃	13.70	14.27	9.00
CaO	11.98	0.72	0.35
Fe ₂ O ₃	10.08	11.32	42.46
N	1.66	1.26	1.05
K ₂ O	1.31	1.73	1.11
Ignition loss	26.05	25.81	17.36
S_{BET} (m ² /g)	31.48	35.88	92.59
Total pore volume (cm ³ /g)	0.017	0.020	0.048

area at 1035 cm^{-1} decreased due to the modification. After TCH adsorption, the peaks of -OH shifted to 3421 cm^{-1} , and 1630 cm^{-1} , respectively, indicating their involvement into the adsorption. The typical peak at 1459 cm^{-1} belonged to C-O stretching in aromatic compound [46] appeared in the spectrum of $\text{Fe}_3\text{O}_4@\text{HAWS}$, indicating the adsorption of TCH on its surface.

AWS had uneven form (Fig. 3c). After treatment by HCl solution, HAWS presented a typical sheet structure (Fig. 3d). Because of the form of Fe_3O_4 , $\text{Fe}_3\text{O}_4@\text{HAWS}$ had a rougher surface with numerous tiny particles and holes following modification by $\text{Fe}^{2+}/\text{Fe}^{3+}$ coprecipitation (Fig. 3e), and the surface of $\text{Fe}_3\text{O}_4@\text{HAWS}$ became smooth as a result of TCH buildup and TCH filling of the pores (Fig. 3d).

Result and Discussion

Effect of Initial Solution pH

Solution pH plays a critical role in the adsorption process due to the fact that it can affect both the surface charge and existing form of TCH. As shown in Fig. 4a), the pH_{pzc} of $\text{Fe}_3\text{O}_4@\text{HAWS}$ was around pH 6.48, indicating its surface was positively charged in the pH range 3-6.48, whereas negatively charged when pH was over 6.5. As shown in Fig. 4b), TCH uptake increased from 18.48 mg/g to 35.84 mg/g as the pH rose from 3-5, and decreased to 7.00 mg/g as the pH increased to 10. In the pH range of 3-5, the major existing forms of TCH were H_4TC^+ and H_3TC , and H_4TC^+ content decreased with the rising pH, leading to the decreased repulsion, whereas, the increased TCH_2^0 content with rising pH resulted to better adsorption because the

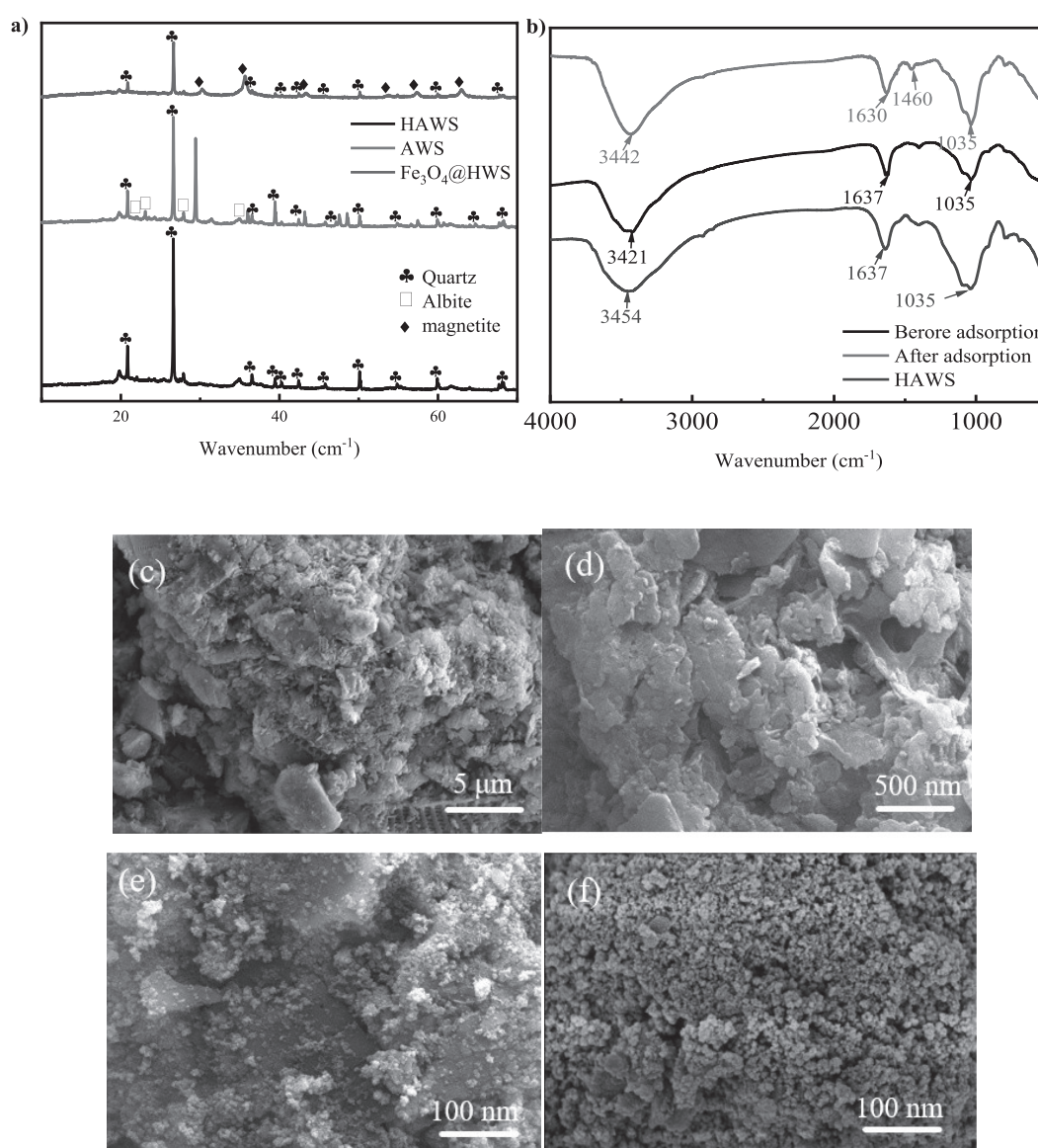


Fig. 3. XRD patterns of AWS, HAWS and $\text{Fe}_3\text{O}_4@\text{HAWS}$ a), FTIR spectra of HAWS and $\text{Fe}_3\text{O}_4@\text{HAWS}$ before and after TCH adsorption b), SEM morphologies of AWS c), HAWS d), $\text{Fe}_3\text{O}_4@\text{HAWS}$ e) and $\text{Fe}_3\text{O}_4@\text{HAWS}$ f).

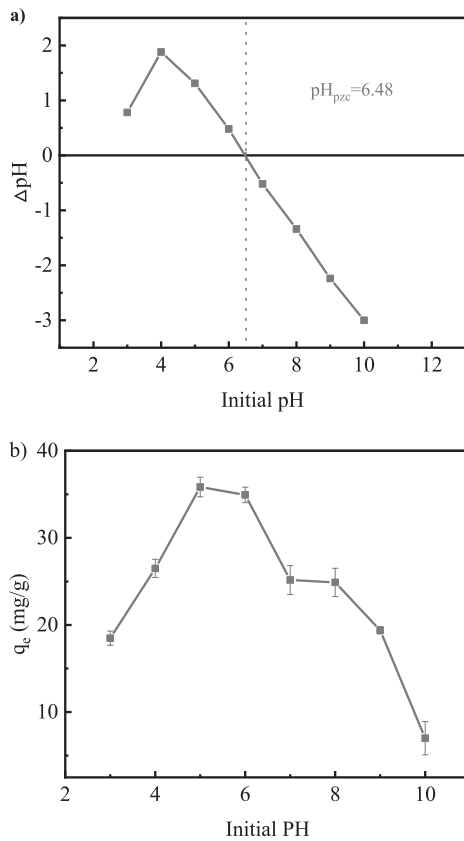


Fig. 4. Determination of pHP_{pzc} a), TCH adsorption by Fe₃O₄@HAWs as a function of initial solution pH b) (C₀ = 20 mg/L, T = 24 h, Temperature = 25°C).

neutral molecular was easier to approach to the surface of Fe₃O₄@HAWs. As the pH increased from 5 to 10 the dominant forms of TCH consisted of TCH₂⁰, H₂TC⁻ and HTC²⁻, and the increasing negatively charged TCH species with rising pH led to the decreased TCH adsorption, and the competition between the OH⁻ and H₂TC⁻ and HTC²⁻ was another reason that weakened TCH adsorption.

Kinetic Study

Pseudo-first order (PFO), pseudo-second order (PSO) and Elovich equations were utilized to analyze the experimental data to further explore the adsorption. The linear forms of the three equations are as follows:

$$\log(q_e - q_t) = \log q_e - \frac{k_1}{2.303} t \quad (2)$$

$$\frac{t}{q_t} = \frac{t}{q_e} + \frac{1}{k_2 q_e^2} \quad (3)$$

$$q_t = \frac{1}{\beta} \ln(\alpha\beta) + \frac{1}{\beta} \ln t \quad (4)$$

Where q_t and q_e (mg/g) was the Cr(VI) uptake quantity at time t and the equilibrium, respectively; k₁ (min⁻¹) and k₂ (g/mg·min) were the PFO and PSO rate constants;

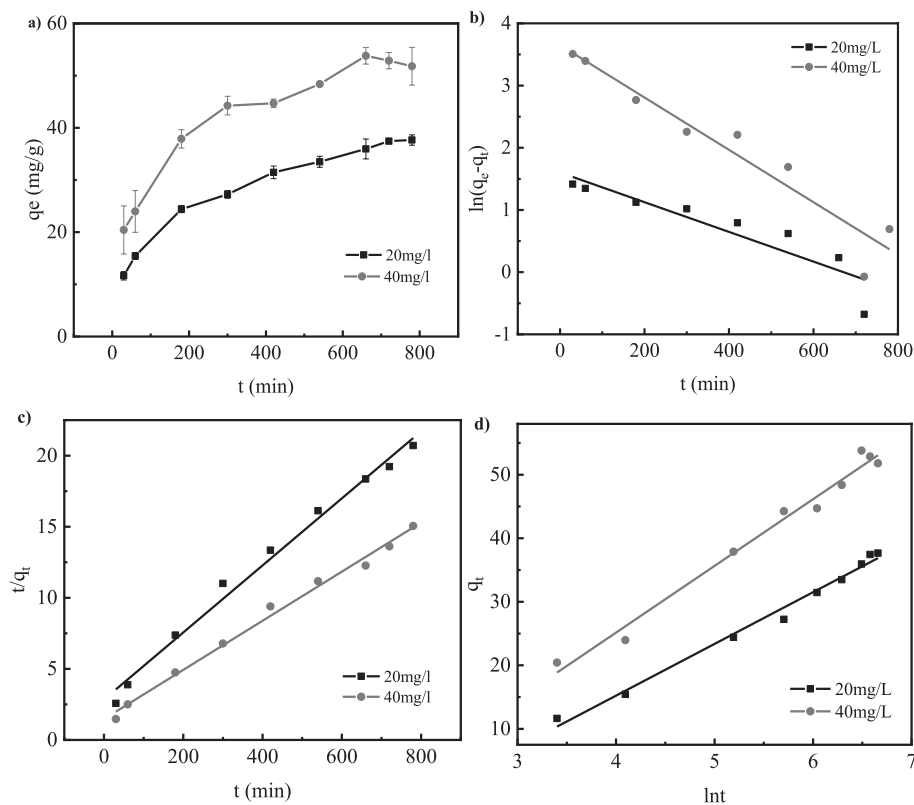


Fig. 5. TCH adsorption as a function of reaction time a), linear fitting plots of pseudo-first order model b), pseudo -second order model c), Elovich model d).

Table 2. Parameters obtained from the three kinetics models for TCH adsorption by Fe₃O₄@HAWs.

C ₀ (mg/L)	PFO model			PSO model			Elovich		
	Q	k ₁	R ²	Q	k ₂	R ²	α	β	R ²
20	4.964	0.0024	0.8395	42.37	0.00019	0.9899	17.325	8.1395	0.9885
40	38.467	0.0042	0.9252	57.80	0.000203	0.9930	16.829	10.496	0.9826

α (mg/g·min) and β (g/mg) were the adsorption rate, and the Elovich constant.

The variation of TCH adsorption as a function of reaction time is shown in Fig. 5a), and Fig. 5(b-d) show the linear fitting results of PFO, PSO and Elovich models. As shown in Table 2, the correlation coefficients (R²) of the PSO equation were highest among those of the three equations, indicating the PSO equation was most suitable to describe the adsorption process, and chemisorption was dominant for the adsorption process.

Isotherm and Thermodynamic Studies

To further understand the adsorption mechanism, five isotherm models, including Langmuir, Freundlich, Temkin, Dubinin-Radushkevich (D-R), and Flory-Huggins (F-H) models were adopted to analyze the experimental data.

Langmuir Model

This model was used to describe the monolayer adsorption on homogeneous surface. The linearized form is shown as:

$$\frac{c_e}{q_e} = \frac{1}{q_m b} + \frac{c_e}{q_m} \quad (5)$$

where b (L/mg) is the Langmuir constant, q_m is the maximum monolayer adsorption capacity (mg/g) at equilibrium. The plots of c_e versus c_e/q_e are shown in Fig. 6b).

Freundlich Model

The model was developed to describe a multilayer adsorption process on a heterogeneous surface, which is shown as:

$$\log q_e = \log k_f + \frac{1}{n} \log C_e \quad (6)$$

where k_f (mg/g) and n are the Freundlich constants related to adsorption capacity and adsorption intensity, respectively. The plots of ln c_e versus ln q_e are shown in Fig. 6c).

Temkin Model

This model assumes a linear decrease in the adsorption heat of molecules with coverage because of the interactions between adsorbate and adsorbent. The linearized form is expressed as:

$$q_e = \frac{RT}{b} \ln A + \frac{RT}{b} \ln c_e \quad (7)$$

$$B = \frac{RT}{b} \quad (8)$$

where R [(8.314 J/(mol K))] is ideal gas constant, T (K) is the reaction temperature, B (J/mol) is the Temkin constant, and A (l/g) is the binding constant.

D-R Model

The D-R model is usually adopted to describe the adsorption with a Gaussian energy distribution. Its linearized form is expressed as:

$$\ln q_e = \ln q_m - k \varepsilon^2 \quad (9)$$

$$\varepsilon = RT \ln \left(1 + \frac{1}{c_e}\right) \quad (10)$$

$$E = \frac{1}{\sqrt{2k}} \quad (11)$$

where k is the D-R constant (mol²/kJ²).

F-H Model

The model was developed to describe the surface coverage degree of adsorbate onto adsorbent, which is shown as:

$$\frac{\theta}{C_0} = K_{FH} (1 - \theta)^{n_{FH}} \quad (12)$$

$$\theta = 1 - \frac{C_e}{C_0} \quad (13)$$

where K_{FH} is equilibrium constant, n_{FH} is the number of adsorbate ions occupying active sites, and θ is the surface coverage degree.

As shown in Fig. 6a), TCH uptakes increased with the rising TCH concentrations at equilibrium

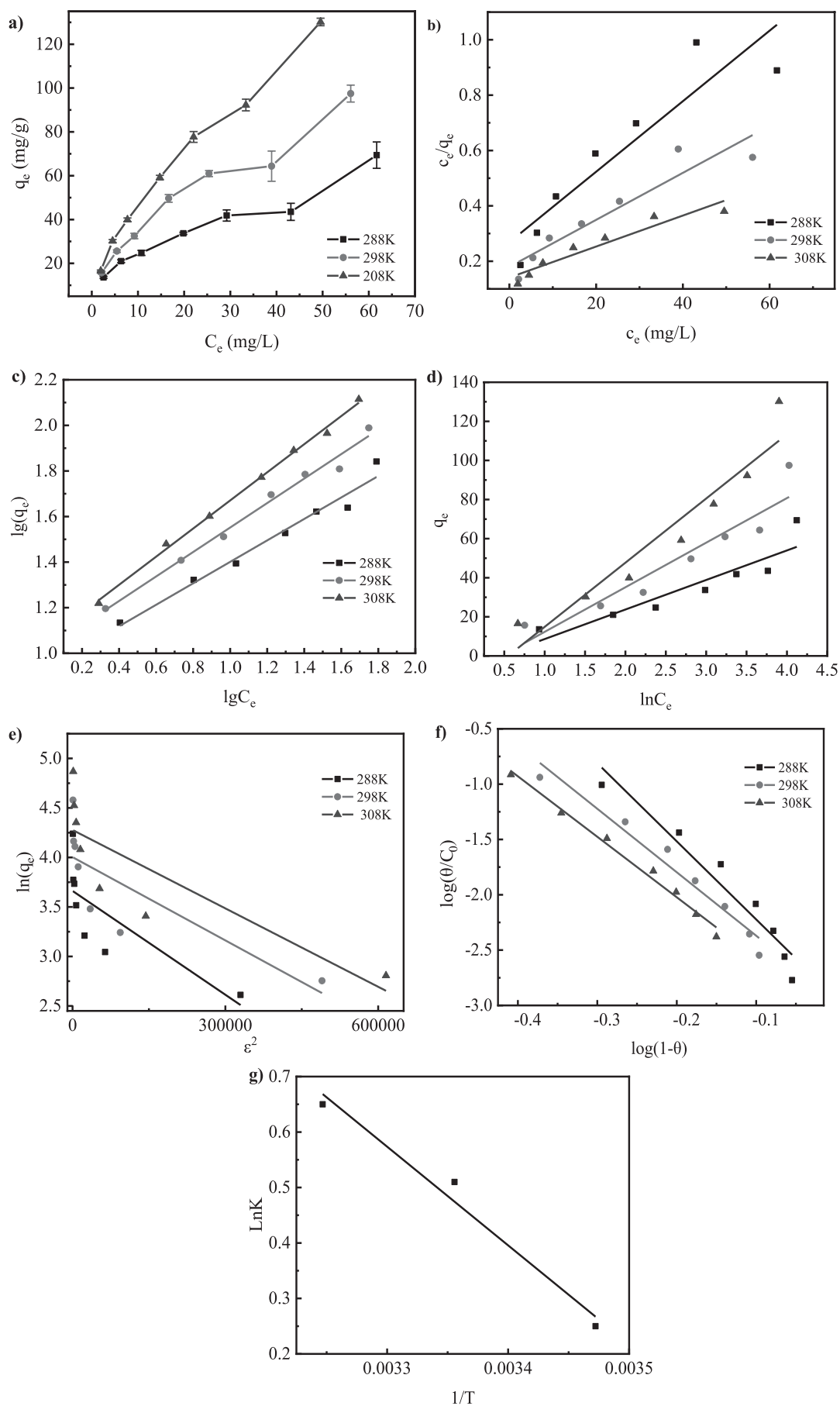


Fig. 6. The relationship between TCH adsorption capacity and its concentration at equilibrium a), the linear fitting by Langmuir b), Freundlich c), Temkin (d), D-R e), and F-H model f), and the relationship between $\ln k$ vs. $1/T$ g).

Table 3. Parameters obtained from the five models for TC adsorption by Fe₃O₄@HAWS.

Isotherm model	Reaction temperature		
	288K	298K	308K
Langmuir Isotherm			
q _m	78.74	117.65	178.57
K _L	0.05	0.047	0.04
R ²	0.847	0.889	0.9163
Freundlich isotherm			
n	2.124	1.862	1.621
K _F	8.515	10.342	11.314
R ²	0.971	0.986	0.997
Timkin isotherm			
A	0.651	0.752	0.821
B	15.112	22.807	32.825
R ²	0.844	0.892	0.894
D-R isotherm			
q _m	17.066	22.233	27.494
E	378.212	422.266	435.206
R ²	0.612	0.646	0.696
F-H isotherm			
n _{FH}	-7.059	-5.737	-5.466
K _{FH}	0.001178	0.001138	0.000766
R ²	0.937	0.962	0.988

due to the further adsorption created by the higher concentration differential between the solution and surface of when the origin TCH concentration was increased. Meanwhile, TCH uptake increased with rising temperature, indicating higher temperature was favorable for the adsorption process. Fig. 6(b-f) shows the linear fitting results using the five models, and the parameters obtained from the models are shown in Table 3, all the three R² values of Freundlich model were highest among the five models, indicating Freundlich model was best to describe the adsorption, and multi-layer adsorption occurred during the adsorption process.

Table 4 Thermodynamic parameters for TC adsorption by Fe₃O₄@HAWS.

T (K)	lnk ₀	ΔG ⁰	ΔH ⁰	ΔS ⁰
288	0.25	-0.655	14.79	53.63
298	0.51	-1.192		
308	0.65	-1.728		

$$\Delta G^0 = -RT \ln k \quad (14)$$

$$\Delta G^0 = \Delta H^0 - T\Delta S^0 \quad (15)$$

where ΔG⁰, ΔS⁰ and ΔH⁰ were the Gibbs free energy change (kJ/mol), the standard entropy change (J/mol·K), and the standard enthalpy change (kJ/mol), respectively. k was the thermodynamic constant (L/g) which could be obtained from intercepts in Fig. 6g).

As given in Table 4, the ΔG⁰ values at the three temperatures were negative, indicating TCH adsorption by Fe₃O₄@HAWS had a spontaneous nature, and the lowering ΔG⁰ values with the rising temperature revealed that higher temperature was favorable for the adsorption process. Furthermore, the ΔH⁰ value was positive, revealing the adsorption process had an endothermic nature.

Conclusions

In this study, AWS was modified by acid activation and Fe²⁺/Fe³⁺ coprecipitation to get an effective Fe₃O₄@HAWS composite for aqueous TCH elimination. The batch static experiments was conducted to test the TCH adsorption performance of the composite. The results showed that TCH uptake was closely related with the solution pH, which increased in the pH range of 3-5, and decreased as the pH increased to 10. The adsorption process fitted the pseudo-second-order equation best among the three kinetics models, and Freundlich equation was better than the other four models to describe the adsorption. The thermodynamics analysis indicated the adsorption process had a spontaneous and exothermic nature. The study offers not only a new solution to the land consumption and environmental contamination caused by the current disposal of AWS, but also a novel insight into the TCH-containing wastewater treatment. The reusability of the composite and its application for industrial wastewater treatment will be investigated in the next study.

Acknowledgment

The authors thank the financial support from the Science and Technology Major Project of Henan Province (Grant No. 161100310700).

Conflict of Interest

The authors declare no conflict of interest.

References

1. DANNER M.C., ROBERTSON A., BEHREND S. V., REISS J. Antibiotic pollution in surface fresh waters:

- Occurrence and effects. *Science of the Total Environment*. **664** (10), 793, **2019**.
2. BOECKELT P.V., BROWER C., GILBERT M., GRENFELL B.T., LEVIN S.A., ROBINSON T.P., TEILLANT A., LAXMINARAYAN R. Global trends in antimicrobial use in food animals. *PNAS*. **112** (8), 5649, **2015**.
 3. SAREMI F., MIROLIAEI M. R., SHAHABI NEJAD M., SHEIBANI H. Adsorption of tetracycline antibiotic from aqueous solutions onto vitamin B6-upgraded biochar derived from date palm leaves. *Journal of Molecular Liquids*. **318** (15), 114126, **2020**.
 4. ZHANG N., CHEN J., FANG Z., TSANG E.P. Ceria accelerated nanoscale zerovalent iron assisted heterogeneous Fenton oxidation of tetracycline. *Chemical Engineering Journal*. **369** (1), 588, **2019**.
 5. SHEN Q., WANG Z., YU Q., CHENG Y., LIU Z., ZHANG T., ZHOU S. Removal of tetracycline from an aqueous solution using manganese dioxide modified biochar derived from Chinese herbal medicine residues. *Environmental Research*. **183**, 109195, **2020**.
 6. QIAN S., QIAO L.N., XU W., JIANG K., WANG Y., LIN H. An inner filter effect-based near-infrared probe for the ultrasensitive detection of tetracyclines and quinolones. *Talanta*. **194** (1), 598, **2019**.
 7. WANG H. Bifunctional copper modified graphitic carbon nitride catalysts for efficient tetracycline removal: Synergy of adsorption and photocatalytic degradation. *Chinese Chemical Letters*. **31** (10), 2789, **2020**.
 8. SUN Y., LI H., LI G., GAO B., YUE Q., LI X. Characterization and ciprofloxacin adsorption properties of activated carbons prepared from biomass wastes by H_3PO_4 activation. *Bioresource Technology*. **217** (15), 239, **2016**.
 9. CHEN T., LUO L., DENG S., SHI G., ZHANG S., ZHANG Y., DENG O., WANG L., JING Z., WEI L. Sorption of tetracycline on H_3PO_4 modified biochar derived from rice straw and swine manure. *Bioresource Technology*. **267**, 431, **2018**.
 10. DAI Y., LIU M., LI J., YANG S., SUN Y., SUN Q., WANG W., LU L., ZHANG K., XU J. A review on pollution situation and treatment methods of tetracycline in groundwater. *Separation Science and Technology*. **55** (5), 1, **2019**.
 11. JAVID A., MESDAGHINIA A., NASSERI S., MAHVI, A.H., ALIMOHAMMADI M., GHARIBI H. Assessment of tetracycline contamination in surface and groundwater resources proximal to animal farming houses in Tehran, Iran. *Journal of Environmental Health Science and Engineering*. **14** (1), 4, **2016**.
 12. CORNO G., YANG Y., ECKERT E., FONTANETO D., FIORENTINO A., GALAFASSI S., ZHANG T., DI CESARE A. Effluents of wastewater treatment plants promote the rapid stabilization of the antibiotic resistance in receiving freshwater bodies. *Water Research*. **158** (1), 114126, **2019**.
 13. ZHANG S., ZHANG Q.Q., LIU Y.S., YAN X. T., ZHANG B., XING C., ZHAO J.L., YING G.G. Emission and fate of antibiotics in the Dongjiang River Basin, China: Implication for antibiotic resistance risk. *Science of the Total Environment*. **712** (10), 136518, **2020**.
 14. XIA J., GAO Y.Q., YU G. Tetracycline removal from aqueous solution using zirconium-based metal-organic frameworks (Zr-MOFs) with different pore size and topology: Adsorption isotherm, kinetic and mechanism studies. *Journal of Colloid and Interface Science*. **590** (15), 495, **2021**.
 15. WANG H., YANG J., YU X.Y., ZHAO G., ZHAO Q.X., WANG N., JIANG Y., JIANG F.Z., HE G., CHEN Y.H. Exposure of Adults to Antibiotics in a Shanghai Suburban Area and Health Risk Assessment: A Biomonitoring-Based Study. *Environmental Science & Technology*. **52** (23), 13942, **2018**.
 16. THEOCHARI N.A., STEFANOPOULOS A., MYLONAS K.S., ECONOMOPOULOS K.P. Antibiotics exposure and risk of inflammatory bowel disease: a systematic review. *Scandinavian Journal of Gastroenterology*. **53** (1), 1, **2018**.
 17. QIAO X., WANG C., NIU, Y.F. N-Benzyl HMTA induced self-assembly of organic-inorganic hybrid materials for efficient photocatalytic degradation of tetracycline. *Journal of Hazardous Materials*. **391** (5), 122121, **2020**.
 18. ZHANG X., LI Y., WU M., PANG Y., HAO Z., HU M., QIU R., CHEN Z. Enhanced adsorption of tetracycline by an iron and manganese oxides loaded biochar: Kinetics, mechanism and column adsorption. *Bioresource Technology*. **320** (A), 124264, **2021**.
 19. SHAO S., HU Y., CHENG J., CHEN Y. Biodegradation mechanism of tetracycline (TEC) by strain *Klebsiella* sp. SQY5 as revealed through products analysis and genomics. *Ecotoxicology and Environmental Safety*. **185** (15), 109676, **2019**.
 20. DEBNATH B., MAJUMDAR M., BHOWMIK M., BHOWMIK K.L., DEBNATH A., ROY D.N. The effective adsorption of tetracycline onto zirconia nanoparticles synthesized by novel microbial green technology. *Journal of Environmental Management*. **261** (1), 110235, **2020**.
 21. ZHOU J., MA F., GUO H.Z. Adsorption behavior of tetracycline from aqueous solution on ferroferric oxide nanoparticles assisted powdered activated carbon. *Chemical Engineering Journal*. **384** (15), 123290, **2020**.
 22. PANDELE A.M., IOVU H., ORBECI C., TUNCEL C., MICULESCU F., NICOLESCU A., DELEANU C., VOICU S.I. Surface modified cellulose acetate membranes for the reactive retention of tetracycline. *Separation and Purification Technology*. **249** (15), 117145, **2020**.
 23. GUO J., HUANG M., GAO P.Q., ZHANG Y., CHEN H.Y., ZHENG S., MU T., LUO X. Simultaneous robust removal of tetracycline and tetracycline resistance genes by a novel UiO/TPU/PSF forward osmosis membrane. *Chemical Engineering Journal*. **398** (15), 125604, **2020**.
 24. YANG G., GAO Q., YANG S., YIN S., CAI X., YU X.G., ZHANG S., FANG Y.X. Strong adsorption of tetracycline hydrochloride on magnetic carbon-coated cobalt oxide nanoparticles. *Chemosphere*. **239** (15), 124831, **2020**.
 25. IPPOLITO J.A., BARBARICK K.A., ELLIOTT H.A. Drinking Water Treatment Residuals: A Review of Recent Uses. *Journal of Environmental Quality*. **40** (1), 1, **2011**.
 26. KAYRANLI B. Adsorption of textile dyes onto iron based waterworks sludge from aqueous solution; isotherm, kinetic and thermodynamic study. *Chemical Engineering Journal*. **173** (3), 782, **2011**.
 27. DASSANAYAKE K.B., JAYASINGHE G.Y., SURAPANENI A., HETHERINGTON C. A review on alum sludge reuse with special reference to agricultural applications and future challenges. *Journal of Waste Management*. **38** (4), 321, **2015**.
 28. KANG S., CHOI J.H., PARK J.G., BAEK K. Pellet adsorbent derived from molasses and dewatered alum sludge for arsenic removal. *Journal of CO₂ Utilization*. **33**, 31, **2019**.
 29. YANG Y., ZHAO Y. Q., BABATUNDE A.O., WANG L., REN Y.X., HAN Y. Characteristics and mechanisms

- of phosphate adsorption on dewatered alum sludge. *Separation and Purification Technology*. **51** (2), 193, **2006**.
30. KEELEY J., JARVIS P., SMITH A. D., JUDD S.J. Coagulant recovery and reuse for drinking water treatment. *Water Research*. **88** (1), 502, **2016**.
 31. LI F., LI G., LIU B., ZHANG X. Enhanced adsorptive removal of oxidation intermediate 1,4-benzoquinone using thermally treated activated carbon fibres. *Desalination and Water Treatment*. **53** (7), 1933, **2013**.
 32. ELANGOVAN C., SUBRAMANIAN K. Reuse of alum sludge in clay brick manufacturing. *Water Supply*. **11** (3), 333, **2011**.
 33. KAISH A.B.M.A., BREESEM A.B., ABOOD M.M. Influence of pre-treated alum sludge on properties of high-strength self-compacting concrete. *Journal of Cleaner Production*. **202** (20), 1085, **2018**.
 34. HOU Q., MENG P., PEI H., HU W., CHEN Y. Phosphorus adsorption characteristics of alum sludge: Adsorption capacity and the forms of phosphorus retained in alum sludge. *Materials Letters*. **229**(15), 31, **2018**.
 35. LEE J.H., JI W.H., LEE J.S., PARK S.S., CHOI K.W., KANG C.U., KIM S.J. A Study of Fluoride and Arsenic Adsorption from Aqueous Solution Using Alum Sludge Based Adsorbent. *Korea Science*. **53** (6), 667, **2020**.
 36. TIE J.X., NIU Y.F., XIAO H., WANG Y.S., DU C.B., ZHANG M., ZHANG J.M., ZHENG Z.H. Performance of Phosphorus Adsorption by Acid-Activated Iron-Based Waterworks Sludge Adsorbent, *Nature Environment and Pollution Technology*. **20** (2), 747, **2021**.
 37. JEON E.K., RYU S., PARK S.W., WANG L., TSANG D. C. W., BAEK K. Enhanced adsorption of arsenic onto alum sludge modified by calcination. *Journal of Cleaner Production*. **176** (1), 54, **2018**.
 38. LIAN J., ZHOU F., CHEN B., YANG M., WANG S., LIU Z., NIU S. Enhanced adsorption of molybdenum (VI) onto drinking water treatment residues modified by thermal treatment and acid activation. *Journal of Cleaner Production*. **244** (20), 118719, **2020**.
 39. TIE J.X., LI W.P., LIU H.Y., HUANG K., MI X., WEI M.H., HOU L.J. Efficient adsorption and reduction of Cr(VI) by a novel polyaniline modified magnetic iron-based waterworks sludge from aqueous solution. *Chemical Engineering Journal*. **21**, 137673, **2022**.
 40. WON S.W., CHOI S.B., YUN Y.S. Performance and mechanism in binding of Reactive Orange 16 to various types of sludge. *Biochemical Engineering Journal*. **28** (2), 208, **2020**.
 41. ZOU C.L., JIANG W., LIANG Y.J., SUN X.H., GUAN Y.Y. Removal of Pb(II) from aqueous solutions by adsorption on magnetic bentonite. *Environmental Science and Pollution Research*. **26**, 1315, **2019**.
 42. ZHU X.D., LIU, Y.C., QIAN F., ZHOU C., ZHANG S.C., CHEN J.M. Preparation of magnetic porous carbon from waste hydrochar by simultaneous activation and magnetization for tetracycline removal. *Bioresource Technology*. **154**, 209, **2014**.
 43. LI H.X., QIU X.S., TANG Y.X. Ash melting behavior by Fourier transform infrared spectroscopy. *Journal of China University Mining and Technology*. **18**, 245, **2008**.
 44. HOCH M., BANDARA A. Determination of the adsorption process of tributyltin (TBT) and monobutyltin (MBT) onto kaolinite surface using Fourier transform infrared (FTIR) spectroscopy. *Collapse-Surface A*. **253** (1-3), 114126, **2020**.
 45. ALFRED G., DEBORAH A.N. Structure of low dielectric constant to extreme low dielectric constant SiCOH films: Fourier transform infrared spectroscopy characterization. *Journal of Applied Physics*. **94** (19), 6697, **2003**.
 46. WEI J., LIU Y.T., ZHU Y.H., LI J. Enhanced catalytic degradation of tetracycline antibiotic by persulfate activated with modified sludge bio-hydrochar. *Chemosphere*. **247**, 125854, **2020**.